CILAMCE 2017

Florianópolis - Santa Catarina - Brazil

THE PROBABILISTIC ANALYSIS OF REINFORCED CONCRETE FRAMES BASED ON THE DAMAGE MECHANICS

Karolinne Oliveira Coelho

Sergio Gustavo Ferreira Cordeiro

Edson Denner Leonel

kocoelho@usp.br; sergio.cordeiro@usp.br; edleonel@sc.usp.br

São Carlos School of Engineering, University of São Paulo.

Av. Trabalhador São Carlense, 400, 13566-590, São Carlos, São Paulo, Brazil.

Julio Flórez-López

julio.lopez@unila.edu.br

Latin-American Institute of Technology, Infrastructure and Territory, Federal University of Latin-American Integration.

Av. Silvio Américo Sasdelli, 85866-000, Foz do Iguaçu, Paraná, Brazil.

Abstract. *The reinforced concrete (RC) is one of the most utilized building materials, which is widely applied in the structural engineering. However, the accurate representation of its complex mechanical behaviour is still a major problem in the structural engineering. Several approaches have been proposed in the literature for addressing this subject. Among them, it is worth citing the damage mechanics. In spite of the accuracy provided by the damage approaches, the mechanical behaviour of the concrete is widely affected by uncertainties, such as concrete cover thickness, geometrical dimensions and mechanical properties. Therefore, the realistic description of the inelastic behaviour of RC structures is only possible through the probabilistic point of view. Thus, this study aims to present a mechanical-probabilistic approach for the modelling of RC frames. The mechanical degradation of the RC is described by the lumped damage model, which represents accurately the concrete cracking and reinforcement yielding. This damage model is coupled to the crude Monte Carlo simulation method, which enables the robust description of failure and safe probabilistic domains. Two applications are presented: one simple supported RC beam and one 2D RC frame. The geometrical and mechanical properties are subjected to the uncertainties. Curves of probability of failure were obtained as well as the probabilistic progressive collapse path.*

Keywords: *Damage mechanics, Structural Reliability, Lumped damage theory, Reinforced concrete.*

1 INTRODUCTION

The reinforced concrete (RC) is one of the world's most common structural system and it is widely used in the construction industry. The coupling of the steel reinforcement bars (rebars) and the concrete provides adequate mechanical strength and durability, with fair costs. Several studies have been developed for the nonlinear RC structural analysis (Mazars & Lemaitre, 1985; Flórez-López, 1998; Lee & Fenves 1998; Park et al., 2010; Oliveira & Leonel, 2013; Liberati et al., 2014; Cordeiro & Leonel, 2015). These models aims at describing the mechanical behavior of RC structures, mainly the nonlinearity caused by its mechanical deterioration.

The mechanical degradation of the RC structures is related to the phenomenon of concrete cracking and the reinforcement yielding. To represent the concrete nonlinear mechanical behaviour, the damage mechanics have been developed. The Kachanov's study, in 1958, was the precursor of the classical damage theory by introducing the concept of effective stress. After the Kachanov (1958), several models were developed and the continuum damage mechanics had significant improvement. Among these models, it is worth mentioning Mazars (1984), which is one of the most utilized damage models due to its simplicity. Although simple, the results obtained with the Mazars theory achieves good accuracy according to the literature (Légeron et al., 2005; Sanches Junior & Venturini, 2007).

However, the continuum damage models, including the Mazars' model, requires a very fine discretization. In addition, the cross section must be divided in small filaments or fibers, which represents, each one, the concrete or the steel mechanical behaviour (Marante & Flórez-López, 2003). Therefore, these models are computationally expensive and could be prohibitive in certain analysis, such as 3D structures and reliability analysis, for instance. These limitations are significant for analysis of complex structures and structural safety.

Over the last years, simplified models have been developed to solve complex inelastic problems without the loss the representativeness. Among them, it is worth citing the lumped damage model, which is based on the idea of coupling the continuum damage theory and fracture mechanics with the plastic hinge concept (Flórez-López et al., 2015). This model includes the damage variable into the plastic hinge, which is generally named as inelastic hinge. Besides simpler, the lumped damage theory have been achieved successfully results, especially in frame structures. Several studies in the literature presents numerical applications in 2D and 3D frames, arches, cyclic loadings, high fatigue, impact loadings or explosion, corrosion analysis and structural reliability (Cipollina et al., 1993; Flórez-López, 1998; Marante & Flórez-López, 2003; Amorim et al., 2014; Coelho, 2017).

Although the nonlinear models should be utilized to represent adequately the mechanical degradation, the RC structural design is usually performed considering the elastic behaviour. Moreover, the structural design aims at obtaining adequate mechanical performance with minimum material consuming, but it does not provide a measure of the structural safety. Thus, the main objective of this study is to determine the failure probability of RC frame structures considering its inelastic mechanical behaviour.

The mechanical modelling is based on the lumped damage theory. Due to the very low computational cost of the mechanical analysis, the lumped damage model is directly coupled with the crude Monte Carlo simulation method, without any metamodeling approach. This strategy enables results with high correspondence with the reality, once the failure analysis is based on the structural response obtained by an accurate mechanical model. Furthermore, for hyperstatic structures, the lumped damage model performs naturally the efforts redistribution during the damage propagation. Thus, it enables obtaining analysis on the failure path and determine the progressive structural collapse configuration, taking into account the uncertainties inherent of the problem.

Two examples of RC structures are showed and the probabilistic inelastic analysis is presented. The first example is an isostatic beam and the second one is a hyperstatic beam. The failure probability curves were showed, as well as the critical path for the hyperstatic case.

2 MECHANICAL MODELLING: THE LUMPED DAMAGE THEORY

The lumped damage mechanics considers a frame structure with deformable elastic elements linked through rigid body joints at the end of each element, as illustrated in Fig. 1. The inelastic effects – the concrete cracking and reinforcement yielding – occurs at the element ends. Thus, the damage index and the plastic rotation variables are added to the body joints, which is generally named inelastic hinges (Flórez-López, 1998).

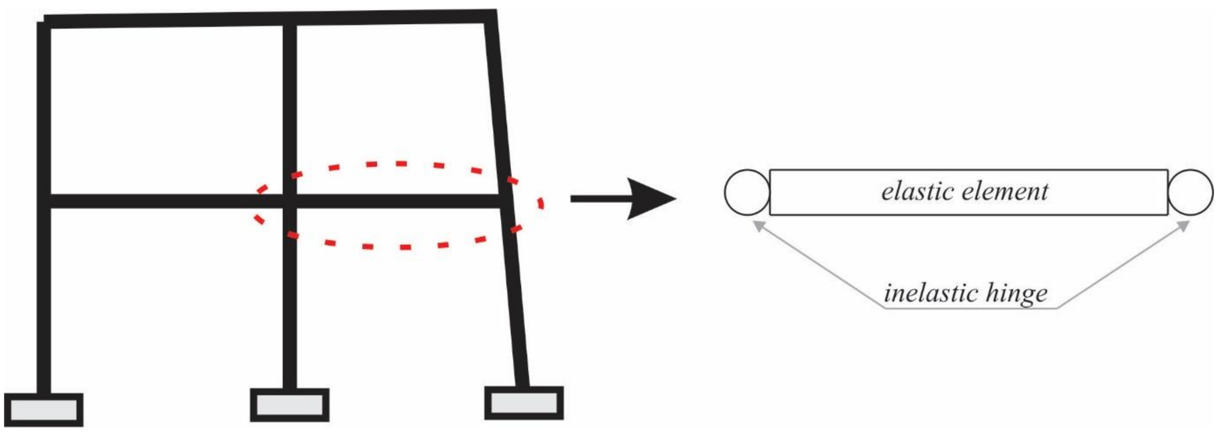

Figure 1. Planar frame structure and the finite element modelled by the lumped damage theory.

The generalized stresses, strains, displacements and damage are obtained by the mechanical analysis described in Fig. 2. The flowchart shows the steps: kinematic relationships, equilibrium and constitutive laws, which in turn contemplates the damage and plasticity relationships.

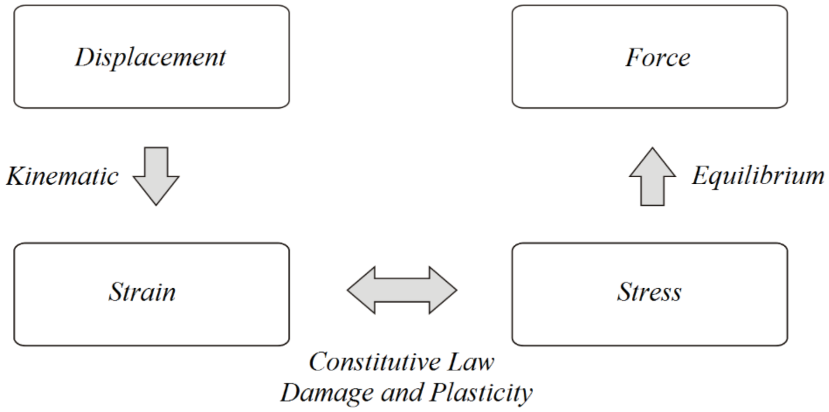

Figure 2. Flowchart with the steps of the lumped damage analysis.

2.1 Kinematic law

Consider a frame element in a 2D space, with two nodes and three degrees of freedom for each node: the horizontal displacement (u), the vertical (w) and the rotation (θ). Its generalized displacement matrix is defined in Eq. (1).

$$\{\boldsymbol{U}\} = \begin{Bmatrix} u_i \\ w_i \\ \theta_i \\ u_f \\ w_f \\ \theta_f \end{Bmatrix}. \tag{1}$$

For the same finite element, the relative rotations on the nodes i and j (ϕ_i and ϕ_j), and the total elongation (δ) compose the generalized strain matrix $\{\boldsymbol{\Phi}\}$, as showed in Eq. (2).

$$\{\boldsymbol{\Phi}\} = \begin{Bmatrix} \phi_i \\ \phi_j \\ \delta \end{Bmatrix}. \tag{2}$$

These generalized displacement and strains, presented in Eq. (1) and (2), respectively, are interrelated by the kinematic relationship, given by the Eq. (3).

$$\{\Delta\boldsymbol{\Phi}\} = [\mathrm{B}_0]\{\Delta\boldsymbol{U}\}. \tag{3}$$

in which $[\mathrm{B}_0]$ is the kinematic transformation matrix, obtained by geometric relations between the deformed and non-deformed situations. For the 2D frame element, the matrix is calculated by the Eq. (4).

$$[\mathrm{B}_0]=\begin{bmatrix} \dfrac{\mathrm{sen}(\alpha)}{L} & -\dfrac{\cos(\alpha)}{L} & 1 & -\dfrac{\mathrm{sen}(\alpha)}{L} & \dfrac{\cos(\alpha)}{L} & 0 \\ \dfrac{\mathrm{sen}(\alpha)}{L} & -\dfrac{\cos(\alpha)}{L} & 0 & -\dfrac{\mathrm{sen}(\alpha)}{L} & \dfrac{\cos(\alpha)}{L} & 1 \\ -\cos(\alpha) & -\mathrm{sen}(\alpha) & 0 & \cos(\alpha) & \mathrm{sen}(\alpha) & 0 \end{bmatrix}. \tag{4}$$

in which α is the angle between the element axis and the horizontal direction.

2.2 Equilibrium law

The equilibrium law is well known in structural analysis. For a structure in equilibrium, the sum of external forces is equal to the sum of internal efforts. Thus, a relationship between the generalized stresses and the external forces matrix is given by Eq. (5), for quasi-static problems.

$$\left[\mathrm{B}_0\right]^T\left\{\boldsymbol{M}\right\}=\left\{\boldsymbol{P}\right\}. \tag{5}$$

in which the generalized stresses $\{\boldsymbol{M}\}$ and external forces matrix $\{\boldsymbol{P}\}$ are defined in Eq. (6) and (7), respectively.

$$\left\{\boldsymbol{M}\right\}=\begin{Bmatrix} m_i \\ m_j \\ n \end{Bmatrix}. \tag{6}$$

$$\left\{\boldsymbol{P}\right\}=\begin{Bmatrix} H_i \\ V_i \\ M_i \\ H_f \\ V_f \\ M_f \end{Bmatrix}. \tag{7}$$

The generalized stresses matrix is composed of the internal efforts: the bending moments at the nodes *i* and *j* (m_i and m_j) and the normal forces *n*. The external forces matrix consists of the horizontal and vertical forces and the bending moment (*H*, *V* and *M*, respectively) applied in each node.

2.3 Constitutive law

The constitutive law associates the generalized stress matrix to the strains through the stiffness or the flexibility matrix. In the present study, it was chosen show the formulation based on the flexibility matrix [F($\boldsymbol{D}$)], as can be seen in Eq. (8) (Flórez-López et al., 2015).

$$\left\{\boldsymbol{\Phi}-\boldsymbol{\Phi}_p\right\}=\left[\mathrm{F}\left(\boldsymbol{D}\right)\right]\left\{\boldsymbol{M}\right\}+\left\{\boldsymbol{\Phi}_0\right\}. \tag{8}$$

in which $\{\boldsymbol{\Phi}_p\}$ is the matrix of the plastic rotations and $\{\boldsymbol{\Phi}_0\}$ is the matrix of initial strains.

By the strain equivalence hypothesis, the flexibility matrix of a damaged element is the sum of the flexibility matrix of the elastic element [F$_0$] and the additional flexibility due to the concrete cracking [C(***D***)], as showed in Eq. (9).

$$\left[\mathrm{F}(\boldsymbol{D})\right]=\left[\mathrm{F}_0\right]+\left[\mathrm{C}(\boldsymbol{D})\right]. \tag{9}$$

Thus, the flexibility matrix is written in terms of the damage parameters, as presented in Eq. (10).

$$\left[\mathbf{F}(\boldsymbol{D})\right]=\begin{bmatrix} \dfrac{L}{3EI\left(1-d_i\right)} & -\dfrac{L}{6EI} & 0 \\ -\dfrac{L}{6EI} & \dfrac{L}{3EI\left(1-d_j\right)} & 0 \\ 0 & 0 & \dfrac{L}{AE} \end{bmatrix}. \tag{10}$$

in which d_i and d_j are the damage indexes related to the nodes i and j.

The damage variables are calculated with the damage evolution law. Moreover, the plastic rotation is obtained with the plastic strain evolution law. Both relationship are presented on the subtopics in sequence.

2.3.1 The damage evolution law

The damage evolution law of the lumped damage model is based on the energy criterion of Griffith, as showed in Florez-López et al. (2015). According to this criterion, the energy release rate during the crack propagation is equal to the derivative of the complementary energy in respect to the damage variables. For the finite element of the study, the strain energy is obtained by the Eq. (11).

$$W_b=\frac{1}{2}\{\boldsymbol{M}\}^T\{\boldsymbol{\Phi}-\boldsymbol{\Phi}_p\}=\frac{1}{2}\{\boldsymbol{M}\}^T\left[\mathrm{F}(\boldsymbol{D})\right]\{\boldsymbol{M}\}+\frac{1}{2}\{\boldsymbol{M}\}^T\{\boldsymbol{\Phi}_0\} \tag{11}$$

The energy release rates for the nodes i and j is defined by the derivative of the Eq. (11) related to the d_i and d_j variables, as shows the Eqs. (12) and (13).

$$G_i=\frac{\partial W_b}{\partial d_i}=\frac{Lm_i^2}{6EI\left(1-d_i\right)}. \tag{12}$$

$$G_j=\frac{\partial W_b}{\partial d_j}=\frac{Lm_j^2}{6EI\left(1-d_j\right)}. \tag{13}$$

The damage evolution law compares the energy release rates with the crack resistance at the inelastic hinge, presented in Eqs. (14) and (15), respectively for the hinges i and j.

$$\begin{cases}\Delta d_i=0,\ \text{se } G_i<R_i \\ G_i=R_i,\ \text{se } \Delta d_i>0\end{cases}. \tag{14}$$

Proceedings of the XXXVIII Iberian Latin-American Congress on Computational Methods in Engineering
P.O. Faria, R.H. Lopez, L.F.F. Miguel, W.J.S. Gomes, M. Noronha (Editores), ABMEC, Florianópolis, SC, Brazil, November 5-8, 2017.

$$\begin{cases} \Delta d_j = 0, \text{ se } G_j < R_j \\ G_j = R_j, \text{ se } \Delta d_j > 0 \end{cases}. \tag{15}$$

Both Eqs. (14) and (15) establish nil damage variation for energy rate values lower than the cracking resistance. On the other hand, when the crack propagation occurs, the energy release rates achieves the crack resistance and energy dissipation in the form of damage propagation is observed.

The cracking resistance is an equation obtained by experimental analysis, as explained in Flórez-López (2015). This equation is a damage function showed in Eq. (16).

$$R(d) = R_0 + q\frac{\ln(1-d)}{1-d}. \tag{16}$$

in which R_0 and q are parameters related to the crack mechanical resistance which depends on the geometrical and mechanical characteristics of the element.

Both values of R_0 and q are obtained from the damage-bending moment relationship. The damage-bending moment curve is determined by making G equal R, obtaining the Eq. (17).

$$m^2 = \frac{6EI(1-d)^2}{L}R_0 + \frac{6qEI}{L}(1-d)\ln(1-d). \tag{17}$$

The initial cracking resistance (R_0) is calculated considering that in the beginning of the crack propagation the bending moment is equal to the cracking moment and the damage is negligible. Thus, the parameter (R_0) is given by the Eq. (18).

$$R_0 = \frac{{M_{cr}}^2 L}{6EI}. \tag{18}$$

in which M_{cr} is the concrete cracking moment.

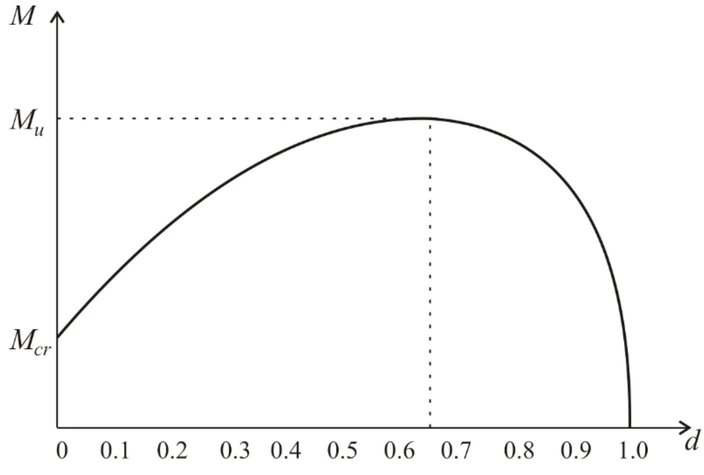

Figure 3. Bending moment as a function of damage.

On the other hand, the parameter q is determined by making the bending moment equal to the ultimate moment and considering the damage equal to the ultimate damage (see Eq. (17)).

Proceedings of the XXXVIII Iberian Latin-American Congress on Computational Methods in Engineering
P.O. Faria, R.H. Lopez, L.F.F. Miguel, W.J.S. Gomes, M. Noronha (Editores), ABMEC, Florianópolis, SC, Brazil, November 5-8, 2017.

The ultimate damage is the point in the damage-bending moment curve (Fig. 3) where the derivative is nil.

2.3.2 The plastic strain evolution law

The plastic strain evolution law for the hinges *i* and *j* is given by the Eqs. (19) and (20), respectively.

$$\begin{cases} d\phi_{p_i} = 0, \text{ se } f_i < 0 \\ f_i = 0, \text{ se } d\phi_{p_i} \neq 0 \end{cases}. \tag{19}$$

$$\begin{cases} d\phi_{p_j} = 0, \text{ se } f_j < 0 \\ f_j = 0, \text{ se } d\phi_{p_j} \neq 0 \end{cases} \tag{20}$$

The yield function is based on the kinematic hardening modelling. Moreover, the evolution of the plastic rotation in RC structures depends of the damage propagation, as shows the Eq. (21).

$$f = \left| \frac{m}{1-d} - c\phi_p \right| - k_0 \tag{21}$$

in which c and k_0 are parameters related to the plasticity.

In the beginning of the rebar yielding behaviour, the yield function is equal to zero, as well as the plastic rotation is negligible. Therefore, k_0 parameter represents the effective yield moment as can be seen in Eq. (22).

$$k_0 = \frac{M_p}{1-d_p} \tag{22}$$

Lastly, when the bending moment reaches its ultimate value, the yield function is also equal to zero. Considering this situation, the parameter c is given by the Eq. (23).

$$c = \frac{1}{\phi_{p_u}} \left(\frac{M_u}{1-d_u} - \frac{M_p}{1-d_p} \right) \tag{23}$$

in which ϕ_{p_u} is the ultimate plastic rotation.

2.4 Cases of continuum damage

The cases of continuum damage (i.e. constant bending moment over the element, such as observed in two point bending test) require a specially scheme. For these cases, the damage is not concentrated at the element ends, but is also present along the entire element length. Therefore, the original formulation of the lumped damage theory is slightly modified.

Coelho et al. (2017) suggest that the element stiffness should be penalized in order to accounting for the mechanical degradation. The stiffness penalization follows the ACI 318-14 recommendations that suggests an analytical procedure to calculate the effective cross-sectional inertia of cracked elements (see Eq. (24)).

Proceedings of the XXXVIII Iberian Latin-American Congress on Computational Methods in Engineering
P.O. Faria, R.H. Lopez, L.F.F. Miguel, W.J.S. Gomes, M. Noronha (Editores), ABMEC, Florianópolis, SC, Brazil, November 5-8, 2017.

$$I_{ef} = \left(\frac{M_{cr}}{m}\right) I_{eq} + \left[1 - \left(\frac{M_{cr}}{m}\right)^3\right] I_{ult} \tag{24}$$

in which the I_{eq} is the cross-section inertia and I_{ult} is the cross-sectional related to the ultimate bending moment, which is given by Eq. (25).

$$I_{ult} = b\bar{d}^3 \left[\frac{1}{2}k^2\left(1 - \frac{k}{3}\right) + n\rho\beta_c\left(k - \frac{\bar{d}'}{\bar{d}}\right)\left(1 - \frac{\bar{d}'}{\bar{d}}\right)\right] \tag{25}$$

in which b is the cross-sectional width, d and d' are the distance between tension and compression rebar and the top surface, respectively, n is the ratio between the Young modulus of the concrete and the steel, k is the neutral axis location and β_c is the coefficient related to the steel rate (see Eq. (26) and Eq. (27))

$$k = \sqrt{(n\rho)^2(1+\beta_c)^2 + 2n\rho\left(1+\beta_c\frac{\bar{d}'}{\bar{d}}\right)} - n\rho(1+\beta_c) \tag{26}$$

$$\beta_c = \frac{(1-n)\rho'}{n\rho} \tag{27}$$

where ρ and ρ' are the rate of tension and compression rebar, respectively.

3 THE PROBABILISTIC MODELLING: APPLICATION OF THE MONTE CARLO SIMULATION METHOD

The reliability methods provide a measure of the structural integrity based on the probabilistic evaluation of the modelling parameters and the failure scenarios. In the reliability problem, a set of parameters are probabilistically considered to modelling their randomness. These variables are named random variables and, with the deterministic parameters, they are used to define the failure scenarios. The failure scenarios are based on the failure modes defined in the structural analysis. For each failure mode, a limit state function is defined, which divides the solution domain in two: the safe and the failure domains. Thus, the probability of failure is the probability of the structural system does not achieve at least one design requirements – mathematically represented by the limit state functions.

In the present study, the limit state functions are defined in terms of loading modelling and resistance capacity, obtained from the mechanical model. The probabilistic problem is solved by using the crude Monte Carlo simulation method. The Monte Carlo simulation (MCS) is a procedure that has been widely used in reliability problems due to its simplicity. This method realizes successive simulations and, in each one, a sampling of random variables is assessed for failure or safe domain. The evaluation of the structural failure is performed according to the limit state function. Therefore, the probability of failure calculated with the MCS method is given by Eq. (28) (Melchers, 1999).

$$P_f = \int_\Omega I[x] f_X(x) dx = \frac{n_f}{n} \tag{28}$$

in which n_f is the number of failures, n is the total number of simulations and $I[x]$ is equal to 1 in the failure domain and nil in the safe domain.

As the number of simulation increases, the probability of failure achieve values with higher accuracy. Consequently, the quality of the results obtained with the MCS technique is linked to the number of simulations. A large amount of simulations could be necessary, principally in problems with small probability of failure (i.e. 10^{-3} or lesser). This leads to high computational cost – one of the principal disadvantages of this method (Santos & Beck, 2015).

However, the major computational efficiency of the lumped damage model allows its coupling with the MCS method, providing results that are more realistic. The MCS enables the failure assessment in each time step for time dependent problems. Moreover, the lumped damage theory performs the efforts redistribution during the damage propagation, even in complex structural systems.

The system reliability concept is important to the reliability analysis of complex structural systems. The modelling based on the system concept identifies and schematizes the failures scenarios as a sequence of components in series and/or in parallel. In the series arrangement, the failure of one component determines the structural failure. On the other hand, for the parallel scheme, only when a set of components failure, the system collapse.

Complex structures can be organized as a sequence of lots of components in series and parallel schemes, systematized as a fault tree. One of the challenges of the fault tree analysis is to determine all the failure paths and calculate the probability of failure associated to each one. Nevertheless, the coupling between the lumped damage model and the MCS method allows the progressive collapse modelling taking into account the uncertainties. Thus, the most probable failure path is obtained directly from the coupled model.

4 APPLICATIONS

The coupled method developed was applied into the mechanical probabilistic analysis of two RC structures: one simple supported beam and one 2D frame. The models were validated by comparing the LDM numerical results with the experimental results and other numerical models available in the literature. Additional details of the validation process is presented in Coelho et al. (2017).

4.1 The simple supported RC beam

The first application is the simple supported beam illustrated in Fig. 4. The RC beam is subjected to two concentrated loads, equally spaced from the supports, creating a region with constant bending moment.

The mean value of the variables is provided by the experimental data (Álvares, 1993), as showed in Table 1. The coefficient of variation (COV) and the probability density function (PDF) is adopted according to Pellizzer (2015). The reinforcement steel consists in CA-50 steel, with yielding and ultimate stress, of 500 MPa and 550 MPa, respectively. The reinforcement design consists in 5 mm diameter stirrups, separated of 12 cm, with concrete cover of 1.5 cm, and longitudinal rebars with 5 and 10 mm diameter. The concrete Young's modulus experimentally measured is 29,200 MPa and the compressive strength is 38 MPa.

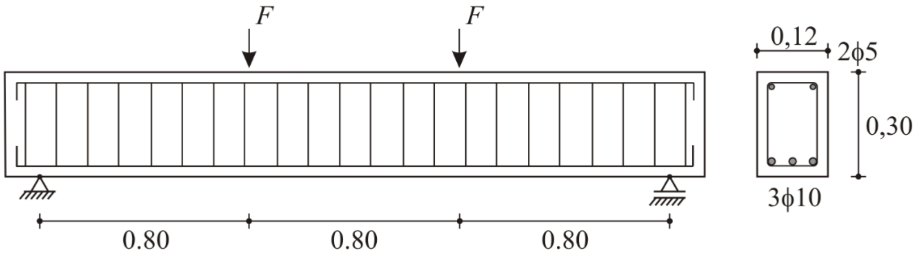

Figure 4. Simple supported beam: reinforcement's design.

Table 1. Random variables: simple supported beam.

Random variable	Mean	COV	PDF
Concrete cover (cm)	1.5	0.15	Normal
Concrete compressive strength (f_c – Mpa)	38.0	0.10	Normal
Reinforcement's yielding stress (f_y – MPa)	500.0	0.05	Lognormal
Reinforcement's ultimate stress (f_{su} – MPa)	550.0	0.05	Lognormal

The incremental-iterative modelling consists in 2.0 kN steps-loading at each time steps, until the rupture of the beam, which occurs around 40 kN (in the deterministic analysis). The COV is 0.10 and the PDF adopted is the Gumbel-max.

The mechanical-probabilistic model achieved values of the failure probability for each loading step, as showed in Fig. 5. According to Fig. 5, the probability of failure has large increase when the mean loading exceeds 32.5 kN, reaching 100% of failure for the loading over 36 kN. This is also verified at the density of failure curve, which shows that the loading between 32.5 kN and 37.5 kN concentrates the major probability of failure.

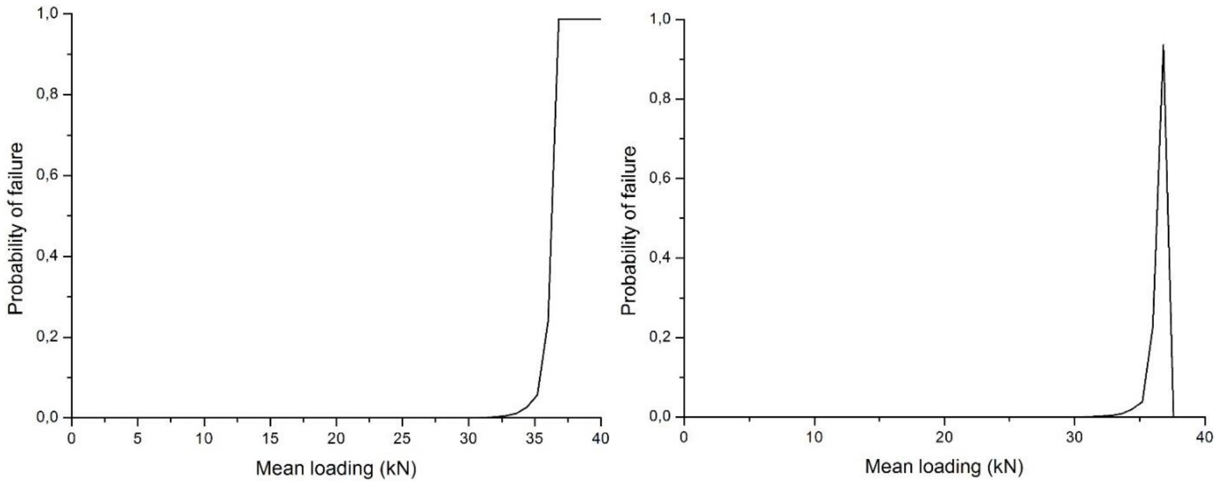

Figure 5. Simple supported beam: probability of failure curve (left) and density of failure (right).

According to the experimental analysis obtained in Álvares (1993) and the numerical analysis of Coelho et al. (2016), when the loading exceeds 32.5 kN occurs the rebar yielding. After this value, the beam presents high displacement values, as showed in Fig. 6.

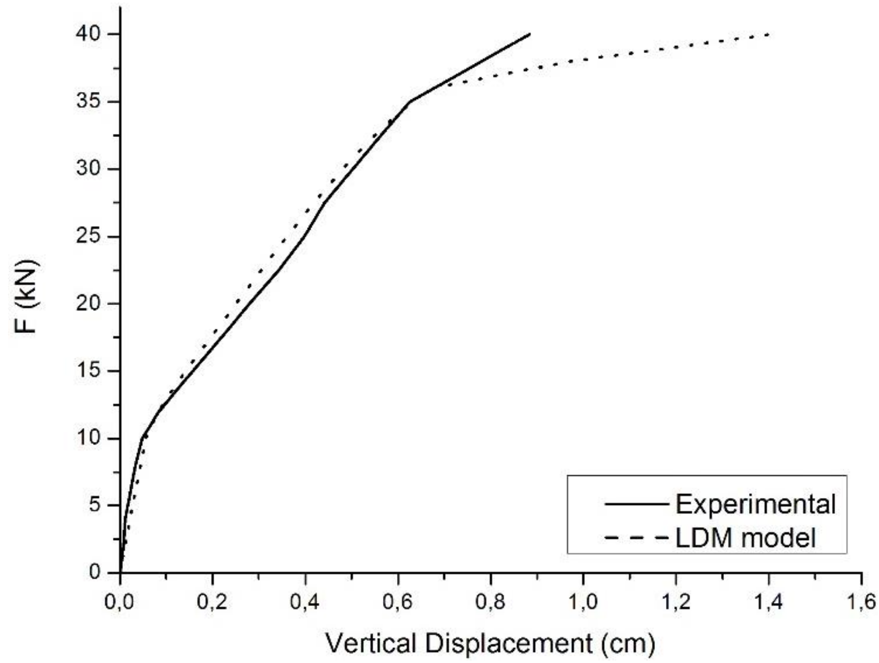

Figure 6. Simple supported beam: Force-displacement curve obtained experimentally by Álvares (1993) and numerically by Coelho (2016).

The JCSS (Diamantidis, 2001) establish target values for probability of failure for different relative costs of measure and consequences of failure. Using the JCSS directives, in the case of large cost of safety measure and minor consequences of failure (i.e. probability of failure around 10^{-3}), the maximum mean loading acceptable is 32 kN, very close to the rebar yielding. Otherwise, if the relative cost of safety measure is small and the failure of the beam causes large consequences (i.e. probability of failure around 10^{-6}), the loading should be below 27 kN.

4.2 The 2D RC frame

The second application is one hyperstatic planar RC frame, as illustrated in Fig. 7. Initially two vertical loads of 700 kN had been applied and afterwards, the horizontal loading was applied until the frame collapse.

Vecchio & Collins (1986) performed experimental analysis of the frame presented in Fig. 7. The mechanical properties provided by the authors are the mean value of the probabilistic problem, as can be seen in Table 2. For the probabilistic analysis, the two vertical loads are deterministic and only the horizontal loading is a random variable. As well as the previous application, the mean horizontal loading was crescent until the frame collapse (around 330 kN). The COV and the PDF were the same of the previous application.

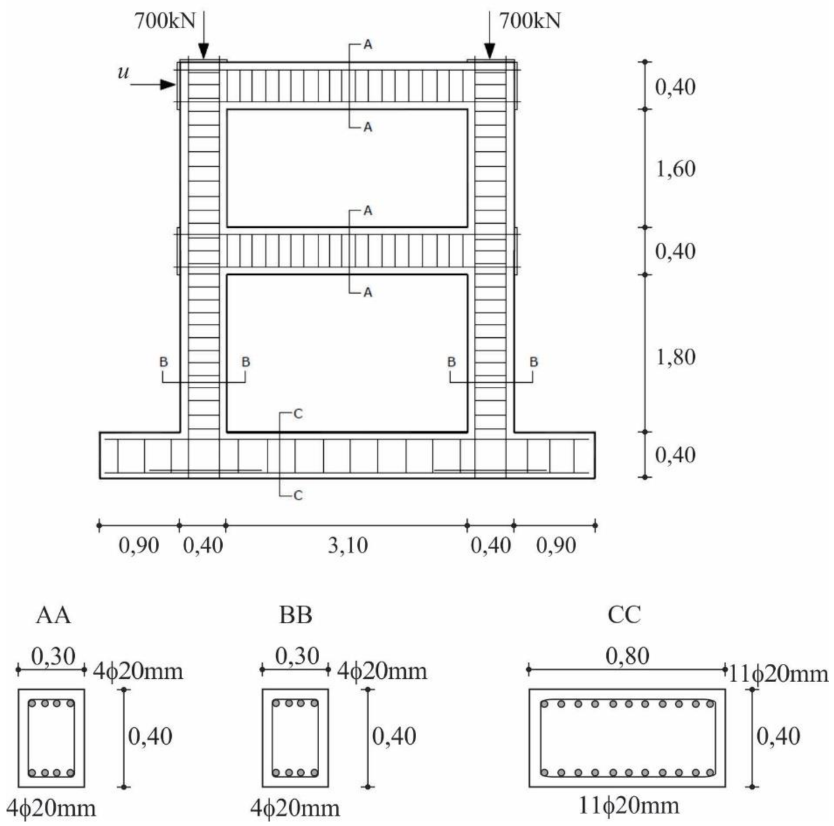

Figure 7. 2D frame: reinforcement's design (Nogueira et al., 2013).

Table 2. Random variables: 2D frame.

Random variable	Mean	COV	PDF
Concrete cover (cm)	3.0	0.15	Normal
Concrete compressive strength (f_c – Mpa)	30.0	0.10	Normal
Reinforcement's yielding stress (f_y – MPa)	418.0	0.10	Lognormal
Reinforcement's ultimate stress (f_{su} – MPa)	598.0	0.10	Lognormal

The mechanical analysis with the lumped damage model required only six finite elements to evaluate the mechanical behaviour, as can be seen in Fig 8, which shows the finite element mesh. The deterministic analysis, presented in Fig 9, shows that the numerical modelling can predict the experimental behaviour with good accuracy. Therefore, even with the simple mesh and the very low computational cost, the results do not lose the representativeness of the mechanical behaviour.

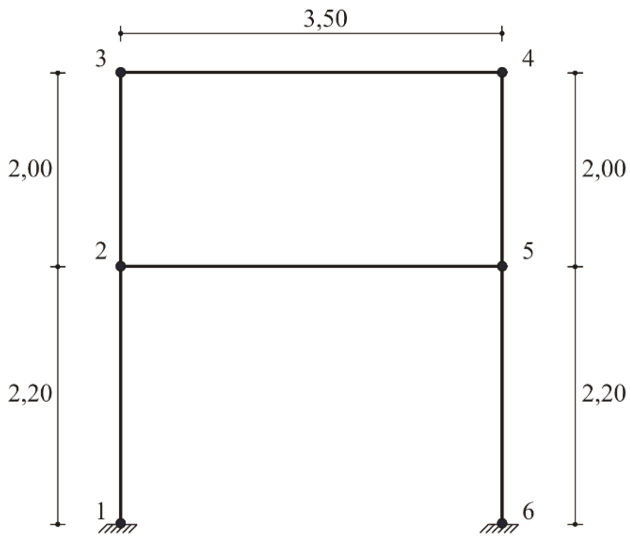

Figure 8. 2D frame: finite element mesh.

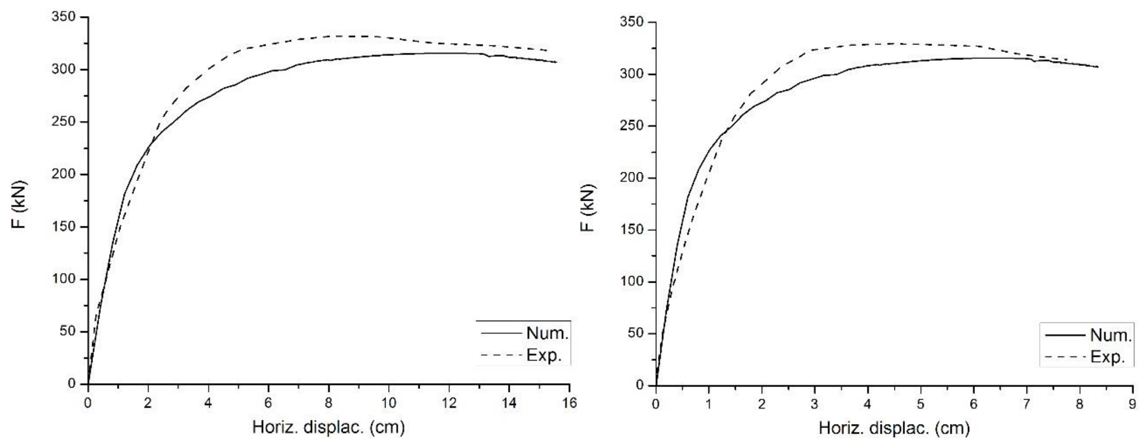

Figure 9. 2D frame: equilibrium trajectory for nodes 3 (left) and 2 (right).

The failure analysis was performed assuming the mean horizontal loading crescent until the structural collapse, which is characterized by the loss of stability. The mechanical modelling considers the efforts redistribution with the increase and damage propagation. The mechanical probabilistic model provides both global and individual probabilities of failure per hinge, and this fact allows a complete structural safety analysis.

Firstly, the global probability of failure is presented in Fig 10, as well as its density of failure. Both curves have significant increase in the probability values after 225 kN. Moreover, the density of failure shows that the mean loading between 225 and 330 kN concentrates the higher values of probability of failure. On the other hand, the values of the probability of failure are lower than the previous example. Such a behaviour is observed because the high hyperstatic degree reduces the global probability of failure, once the structural system is composed of parallel components: only the failure of all components in parallel leads to the structural collapse.

Proceedings of the XXXVIII Iberian Latin-American Congress on Computational Methods in Engineering
P.O. Faria, R.H. Lopez, L.F.F. Miguel, W.J.S. Gomes, M. Noronha (Editores), ABMEC, Florianópolis, SC, Brazil, November 5-8, 2017.

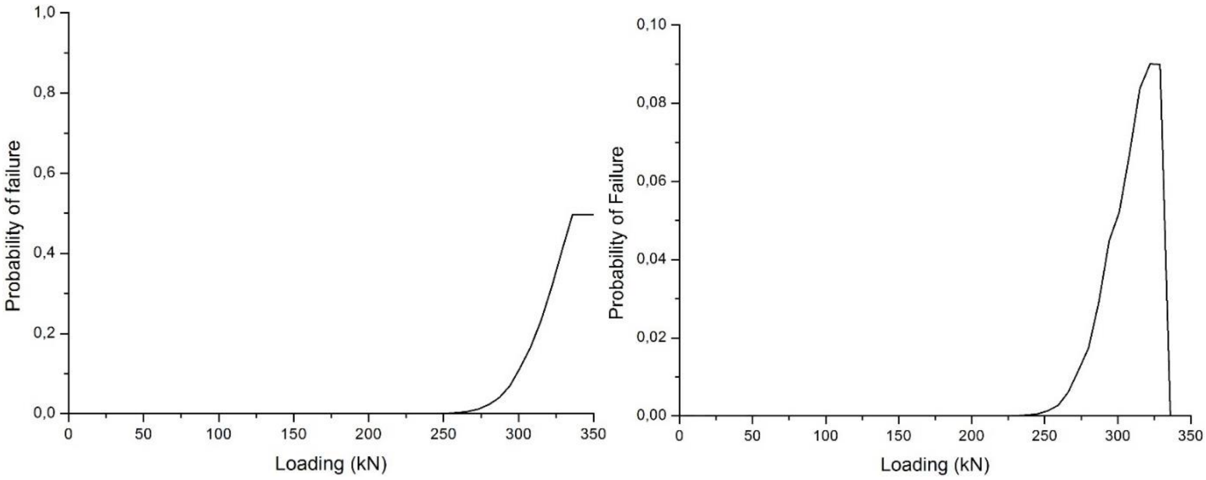

Figure 10. 2D frame: probability of failure (left) and density of failure (right).

One important result of the structural safety analysis of hyperstatic structures is the critical path determination. For this purpose, the Fig. 11 shows the individual probability of failure per hinge for two mean horizontal loading values: 245 kN and 350 kN. In the first case, the individual probabilities of failure are around 10^{-5}, except for the fixed support, which concentrates the higher values for the both loading cases.

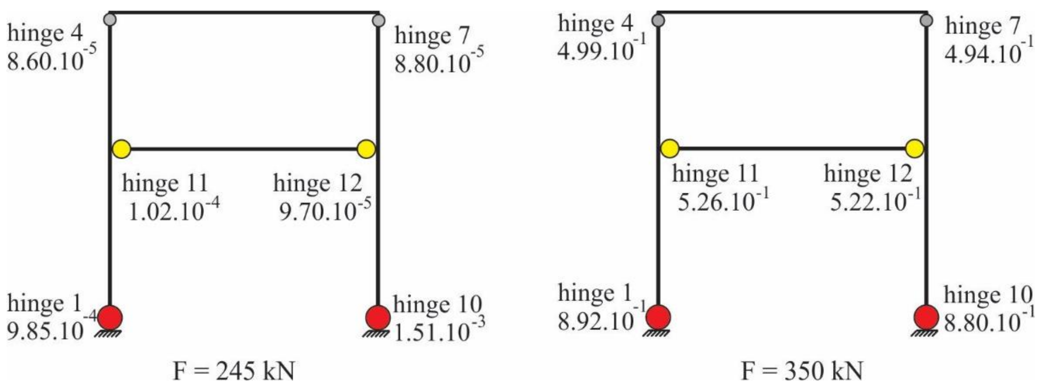

Figure 11. 2D frame: Probability of failure maps for 245 kN (left) and 350 kN (right).

According to the Fig. 11, we can conclude that the two first failures are related to the fixed support: hinges 1 and 10. Afterwards, the sequence of failure is composed of hinges 11 and 12, followed by the top of the columns (hinges 4 and 7). The probability of failure map allows the visualization of the progressive collapse path. It is an important tool in structural repair and maintenance that shows the regions with higher concrete cracking, which are more exposed to deterioration mechanisms, such as reinforcement corrosion, and are more susceptible to failure. Lastly, the individual probability of failure curves are shown in Fig. 12, for the hinges 1, 4 and 11. All graphs present significant growth after 250 kN, and the curve relative to the hinge 1 concentrates the higher values.

Proceedings of the XXXVIII Iberian Latin-American Congress on Computational Methods in Engineering
P.O. Faria, R.H. Lopez, L.F.F. Miguel, W.J.S. Gomes, M. Noronha (Editores), ABMEC, Florianópolis, SC, Brazil, November 5-8, 2017.

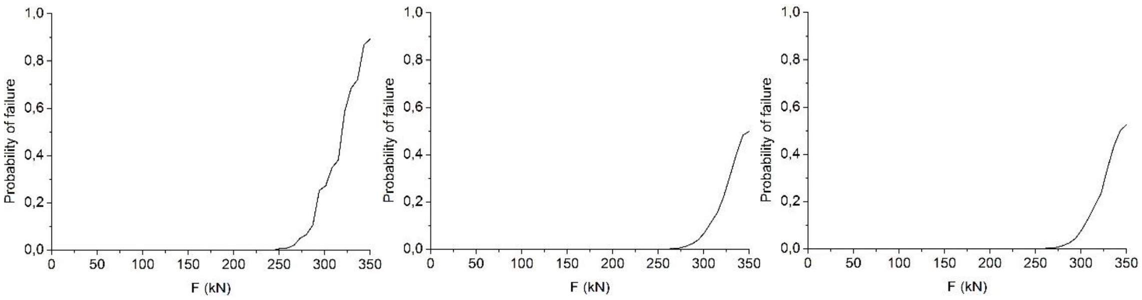

(a) (b) (c)

Figure 12. 2D frame: Individual probability of failure for: (a) hinge 1 (left), (b) hinge 4 (in the middle) and (c) hinge 11 (right).

Considering the JCSS directives in the scope of the global probability of failure, the maximum acceptable mean loading is 259 kN for minor consequences of failure and large costs of safety measure. Otherwise, if the same analysis is performed on the local failure scope, the maximum mean load value is 220 kN (i.e. the probability of the hinges 1 or 10 collapse is around 10^{-3}). The horizontal load value of 220 kN seems more appropriated, since the value of 259 kN leads to damage index around 0.30 for the hinges 1 and 10. This condition characterized the reinforcement yielding at the fixed support, which is unexpected for an analysis based on the service life and structural performance.

On the other hand, the large consequences of failure and small costs of safety measure leads to the mean horizontal loading of 217 kN, if we considered only the global failure analysis. For local failure analysis, this value reduces to 180 kN, which is significantly lower than the collapse loading condition.

5 CONCLUSIONS

The present study aimed to perform probabilistic analyses of the RC structures. For this purpose, a computational framework was developed, which couples the lumped damage theory with the crude Monte Carlo simulation technique. Due to the computational efficiency of the lumped damage model, the coupling with the MCS method was successful achieved. The coupled model did not require any metamodeling analysis and the mechanical modelling also redistributes the efforts as the damage propagates. For these reasons, realistic results were obtained, even for complex structures with high hyperstatic degree.

Two applications were illustrated in the present study: one simple supported RC beam and one hyperstatic RC frame. The probability of failure curves were obtained for several mean loading values, as well as load values were suggested based on the JCSS recommendations.

The main contribution of the present study is the determination of the critical path based on the progressive collapse of hyperstatic structures. Thus, the progressive structural collapse configuration of the 2D frame was determined taking into account the uncertainties. Moreover, the local probabilities of failure per hinge were presented in a failure map, which is especially useful in structural repair analysis.

ACKNOWLEDGEMENTS

The authors would like to thank the financial support provided by the Brazilian National Council for Scientific and Technological Development (CNPq) for this research project.

REFERENCES

ACI Committee. (2008). *Building code requirements for structural concrete (ACI 318-08) and commentary*. American Concrete Institute.

Álvares, M. D. S., 1993. *Estudo de um modelo de dano para o concreto: formulação, identificação paramétrica e aplicação com o emprego do método dos elementos finitos.* Master degree thesis, Universidade de São Paulo/São Carlos.

Amorim, D. L. D. F., Proenca, S. P., & Florez-Lopez, J., 2014. Simplified modeling of cracking in concrete: Application in tunnel linings. *Engineering Structures*, vol. 70, pp. 23-35.

Cipollina, A., López-Inojosa, A., & Flórez-López, J., 1995. A simplified damage mechanics approach to nonlinear analysis of frames. *Computers & Structures*, vol. 54, n. 6, pp. 1113-1126.

Coelho, K. O., 2017. Modelos numéricos aplicados à modelagem probabilística da degradação mecânica do concreto e corrosão de armaduras. Master degree thesis, Universidade de São Paulo/São Carlos.

Coelho, K. O., Leonel, E. D., & Flórez-López, J., 2017. The Mechanical Behavior Modeling of Reinforced Concrete Structures by the Lumped Damage Model. In: Robinson, S. ed., *Reinforced Concrete: Design, Performance and Applications*, pp. 49-68. Nova Science Publishers.

Cordeiro, S. G. F., Leonel, E. D., & Beaurepaire, P., 2017. Quantification of cohesive fracture parameters based on the coupling of Bayesian updating and the boundary element method. *Engineering Analysis with Boundary Elements*, vol. 74, pp. 49-60.

Diamantidis, D. (ed.), 2001. *Report 32: Probabilistic Assessment of Existing Structures-A publication for the Joint Committee on Structural Safety (JCSS),* vol. 32. RILEM publications.

Flórez-López, J., 1998. Frame analysis and continuum damage mechanics. *European Journal of Mechanics-A/Solids*, vol. 17, n. 2, pp. 269-283.

Flórez-Lópes, J., Marante, M. E., & Picón, R., 2015. *Fracture and Damage Mechanics for Structural Engineering of Frames: State-of-the-Art Industrial Applications*. IGI global.

Kachanov, L. M., 1958. *Time of the Rupture Process under Creep Conditions*, Izy Akad. Nank SSR Otd Tech Nauk, vol. 8, pp. 26-31.

Lee, J., & Fenves, G. L., 1998. Plastic-damage model for cyclic loading of concrete structures. *Journal of engineering mechanics*, vol. 124, n. 8, pp. 892-900.

Légeron, F., Paultre, P., & Mazars, J., 2005. Damage mechanics modeling of nonlinear seismic behavior of concrete structures. *Journal of Structural Engineering*, vol. 131, n. 6, pp. 946-955.

Liberati, E. A., Nogueira, C. G., Leonel, E. D., & Chateauneuf, A., 2014. Nonlinear formulation based on FEM, Mazars damage criterion and Fick's law applied to failure assessment of reinforced concrete structures subjected to chloride ingress and reinforcements corrosion. *Engineering Failure Analysis*, vol. 46, pp. 247-268.

Marante, M. E., & Flórez-López, J., 2003. Three-dimensional analysis of reinforced concrete frames based on lumped damage mechanics. *International Journal of Solids and Structures*, vol. 40, n. 19, pp. 5109-5123.

Mazars, J., 1984. Application de la mechanique de l'endommagement au comportement non lineaire et à la rupture du béton de structure. PhD thesis, Université Paris 6/Paris.

Mazars, J., & Lemaitre, J., 1985. Application of continuous damage mechanics to strain and fracture behavior of concrete. In: *Application of Fracture Mechanics to Cementitious Composites*, pp. 507-520. Springer Netherlands.

Nogueira, C. G., Venturini, W. S., & Coda, H. B., 2013. Material and geometric nonlinear analysis of reinforced concrete frame structures considering the influence of shear strength complementary mechanisms. *Latin American Journal of Solids and Structures*, vol. 10, n. 5, pp. 953-980.

Oliveira, H. L., & Leonel, E. D., 2013. Cohesive crack growth modelling based on an alternative nonlinear BEM formulation. *Engineering Fracture Mechanics*, vol. 111, pp. 86-97.

Park, K., Paulino, G. H., & Roesler, J., 2010. Cohesive fracture model for functionally graded fiber reinforced concrete. *Cement and concrete research*, vol. 40, n. 6, pp. 956-965.

Pellizzer, G. P., Leonel, E. D., & Nogueira, C. G., 2015. Influence of reinforcement's corrosion into hyperstatic reinforced concrete beams: a probabilistic failure scenarios analysis. *Revista IBRACON de Estruturas e Materiais*, vol. 8, n. 4, pp. 479-490.

Sanches Junior, F., & Venturini, W. S., 2007. Damage modelling of reinforced concrete beams. *Advances in Engineering Software*, vol. 38, n. 8, pp. 538-546.

Santos, K. R. dos, & Beck, A. T., 2015. A benchmark study on intelligent sampling techniques in Monte Carlo simulation. *Latin American Journal of Solids and Structures*, vol. 12, n. 4, pp. 624-648.

Vecchio, F. J., & Collins, M. P., 1986. The modified compression-field theory for reinforced concrete elements subjected to shear. *ACI Journal*, vol. 83, n. 2, pp. 219-231.